Applied Physics Express

LETTER • **OPEN ACCESS**

Spatial and temporal thermal management of a spintronic terahertz emitter

To cite this article: Gabriel Gandubert *et al* 2024 *Appl. Phys. Express* **17** 083001

OPEN ACCESS

Applied Physics Express 17, 083001 (2024) LETTER

https://doi.org/10.35848/1882-0786/ad6955

Spatial and temporal thermal management of a spintronic terahertz emitter

Gabriel Gandubert[1], Joel Edouard Nkeck[1], Xavier Ropagnol[1,2], Denis Morris[3], and François Blanchard[1*]

[1]École de Technologie Supérieure (ÉTS), Montréal, QC, H3C 1K3, Canada
[2]INRS—EMT Institut National de Recherche Scientifique, Varennes, QC, J3X 1P7, Canada
[3]Université de Sherbrooke, Sherbrooke, QC, J1K 2X9, Canada

*E-mail: francois.blanchard@etsmtl.ca

Received June 29, 2024; revised July 25, 2024; accepted July 29, 2024; published online August 12, 2024

This work presents methods for addressing undesirable thermal effects induced by the pump beam of an oscillator laser to improve the efficiency of a terahertz (THz) spintronic emitter. We explore two approaches: spatial distribution of pump energy using a 2D lens array and temporal modulation of the pump duty cycle. Optimizing the spatial distribution approximately doubles the THz signal by increasing local heat dissipation, delaying the saturation limit. Similarly, temporal spreading of pump pulses by adjusting the duty cycle allows greater thermal relaxation within the heterostructure, enhancing the overall efficiency of THz wave generation. © 2024 The Author(s). Published on behalf of The Japan Society of Applied Physics by IOP Publishing Ltd

Terahertz (THz) waves find applications in diverse fields such as biochemistry,[1)] medical diagnosis,[2)] quality control,[3)] communication,[4)] security,[5)] and more. However, generating electromagnetic waves in the THz band (0.1 to 10 THz) presents challenges and has lacked efficient sources and detectors for decades.[6)] There are many methods of generation, with two popular approaches, namely optical rectification[7)] using organic[8)] or non-centrosymmetric inorganic crystals,[9)] and photoconductive antennas.[10)] Recently, the development of a broadband 2D spintronic THz emitter (STE) presents an interesting alternative to standard methods for the efficient generation of THz waves.[11)] While spintronic-based methods provide sufficient THz power for a variety of applications, their pump conversion efficiency typically remains relatively low (<1%),[12)] making any potential improvement crucial for THz development.

Recent improvements to STEs include emitter material composition,[13)] manufacturing processes,[14)] modulation techniques,[15)] cooling methods,[16)] optical pump confinement[17)] and pump beam characteristics.[18,19)] Since STE is based on ultra-fast demagnetization by transferring energy to the emitter,[20)] its maximum emission efficiency saturates through thermal heating.[16)] The impact of the pump on the efficiency of the STE has been reported, including changes in beam size to increase the THz radiation for large-area STEs.[18,19)] Laser repetition rate has also recently been reported to have an impact on the destruction threshold of STEs which is currently known to be dependent on pump fluence for kHz amplified lasers.[13,16,21)] However, the destruction threshold is also dependent on the average power for CW and MHz oscillator lasers with a reported transition threshold around 4 MHz for a fiber-tip emitter.[22)] From this study, we know that high repetition rate lasers are more damageable to the spintronic emitter, thus reducing the maximum THz generation limit. In this study, thermal dissipation on the STE surface is achieved by spatial and temporal handling of the pump beam derived from a ytterbium (Yb) laser oscillator. Spatial management of the pump beam is ensured using a 2D lens array to distribute the energy into multiple generation points on the emitter, resulting in up to a twofold increase in amplitude compared to a standard spherical lens for a similar pumping area. Temporal modulation is accomplished by modulating the duty cycle of the pump beam to create pulse bursts of optimal duration to increase THz generation. Finally, the THz response of a CdTe emitter is used to compare the expected response of different burst durations with the STE.

The spintronic device used in this work has been detailed previously for a similar configuration generating THz pulse trains.[4)] In this experiment, the size of the spintronic THz emitter (STE) was reduced to a $1 \times 1\ \mathrm{cm}^2$ area. The experimental setup is depicted in Fig. 1(a). The laser used is the Chameleon Discovery NX with total power control (TPC), a femtosecond oscillator from Coherent, Inc., which is a Yb oscillator coupled to an optical parametric oscillator (OPO). Consequently, we have two laser beam lines at an 80 MHz repetition rate, one fix that delivers 150 fs pulses at a 1.040 μm wavelength and a tunable source that delivers 100 fs pulses from 660 nm to 1320 nm. Both outputs are modulable by an internal acousto-optic modulator (AOM), which can be m`odulated up to 1 MHz with various waveforms. The fixed output can deliver up to 4.4 W and is used exclusively as the pump beam for THz emission. The tunable output can generate up to 3 W of power at 800 nm, which was reduced to 10 mW to be used as the probe signal for the LT-GaAs detector antenna from TeraVil company. Modulation of the optical pump output is produced by a square wave at 30 kHz for experiments to assess the effect of spatial distribution on the emission saturation level. A rectangular wave with different duty cycles from 5% to 50% was used for measurements aimed at evaluating the effect of temporal modulation on the emission saturation level.

To study the effect of spatial distribution on the STE saturation level, two types of illumination conditions were used: conventional illumination using a spherical lens, and illumination using a 2D lens array, for similar total surface areas. For each illumination condition, the position of the transparent polymer X lens (TPX) was adjusted to optimize the THz signal detected by the PCA detector. The effective illumination area on the emitter was measured by

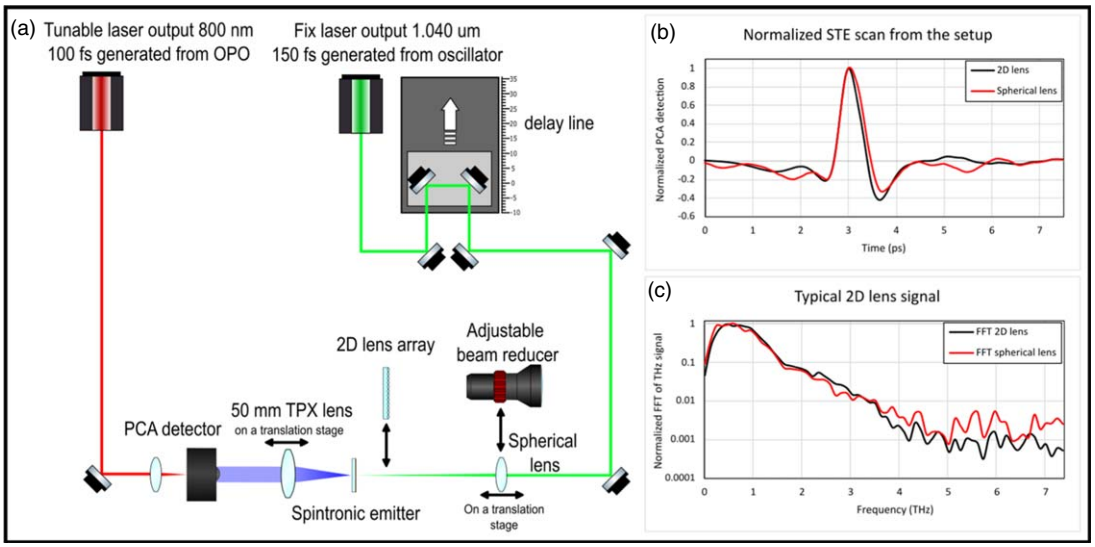

Fig. 1. Experimental setup of the system (a) for the generation via STE by a spherical lens/2D lens matrix and the detection via photoconductive antennas of THz waves. (b) Time variation of the THz field generated by the STE when pumped with a 2D lens matrix (nine spots) and the spherical lens (0.01 mm^2) and (c) their respective spectra.

imaging the STE surface using a wedge, a microscope objective, and a CCD camera. The detected THz signal for both pumping methods exhibited similar waveforms and spectral distributions, as shown in Figs. 1(b)–1(c). These results are an indication that the illumination conditions explored here do not affect the generation mechanism at play.

The characterization of the STE is done through a THz field dependence as a function of optical power in both cases and compared its different saturation levels. As the STE tends to be easily damaged by the optical pump beam,[13,22] we took care to avoid damaging the STE and confirm its integrity by measuring its thermal hysteresis cycle. The saturation point is determined by the maximal THz generation achieved by the emitter before the peak-to-peak THz signal reduces for a higher pump laser fluence. By taking a discreet number of points, the saturation point is determined by the zero crossing of the derivative of the peak-to-peak graph.

For the temporal modulation experiment, no adjustment was required in the detection arm when transitioning between the two pumping methods. Thus, an off-axis mirror was used with the PCA instead of a TPX lens, as shown in Fig. 1(a). For this experiment, the beam was focused on the emitter surface onto a spot area equal to 0.46 mm^2. Considering that the lock-in amplifier filters out all frequencies other than the fundamental modulation frequency at 30 kHz, we need to correct the measured signal to account for the variation in the frequency content of the modulation signal when the duty cycle changes. The correction factor is inversely proportional to $\sin(DC\cdot\pi)$, where DC corresponds to the duty cycle in the range [0, 0.5]. The behavior of the corrected amplitude of the THz beam generated as a function of the wave modulation duty cycle was obtained for two types of sources: the spintronic emitter and a CdTe crystal. Unlike spintronic emitters, CdTe crystals are robust emitters, based on the optical rectification mechanism, which should not present any saturation effect under the excitation conditions explored in this work.[23,24] To evaluate the effect of pulse relaxation, a previous study considered the thermal dissipation of the metallic heterostructure as a uniform plane (of surface A and thickness Δx) and the thermal impact of multiple consecutive pulses in time by Fourier's law.[21] Considering the conductivity of the metal layers (C), the thermal dissipation factor (k), the room temperature (T_R), and the increase in temperature for the nth pulse (P), the theoretical equation is:

$$T_{0,n+1} = T_R + \left(T_{0,n} + \frac{P}{C}\right)e^{-kAt/C\Delta x} \quad (1)$$

The limit of this equation is linked to the thickness of the emitter for electron scattering in a metallic thin film,[25] the heat conductivity of the materials used for the heterostructure, and the high repetition rate. In another study, the saturation limit of an STE pumped with a high repetition rate laser changed from a pulse energy dependence to an average power dependence for a repetition rate over 4 MHz.[22] Therefore, due to this identified limitation, the thermal relaxation model needs further tests in the high repetition rate regime to reduce the impact of short pulse bursts.

For the 2D lens, five illumination conditions were considered, with 1, 4, 9, 16, and 25 micro-spots corresponding to areas of 0.00151, 0.00776, 0.0241, 0.085 and 0.127 mm^2, respectively. With the spherical lens, five equivalent areas with spot sizes ranging from 0.00133 to 0.178 mm^2 were tested. Figures 2(a)–2(j) show the image of the optical spot for the 2D lens [(a)–(e)] and the spherical lens [(f)–(j)]. When using the 2D lens, we noticed that the amplitude distribution between the different spot sizes is not uniform as shown in Fig. 2(k). Figure 2(m). We attribute this observation to the Gaussian intensity distribution of the laser beam, which is only enlarged by the beam expander. The area of each spot is estimated from the effective diameter measured at half-height of the intensity profile, and the total illuminated area is obtained from the sum of these areas. This total surface was compared to the one calculated using the effective diameter of the beam spot obtained with the spherical lens. Note that the diameter of each beam spot produced by the 2D lens is independent of the size of the optical beam illuminating that lens and is equivalent to the smallest spot size obtained with the spherical lens when the STE is in focus [Fig. 2(f)].

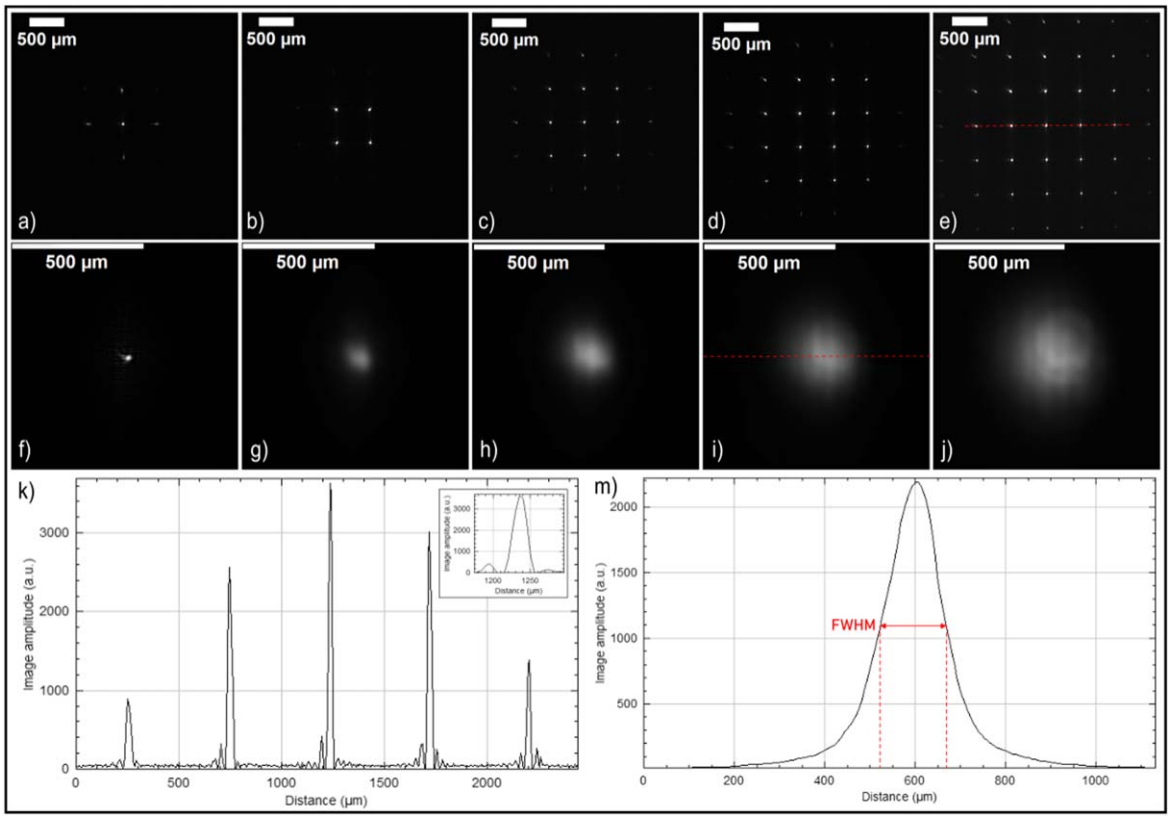

Fig. 2. Spot size images for (a)–(e) 2D matrix lens and for (f)–(j) spherical lens. (k) Spot profiles extracted from the red line in (e) and (m) for 2D and spherical lens beams, respectively.

For each pump distribution, the pump power was scaled until the THz signal decreased. This method was first validated by a power-dependent hysteresis experiment illustrated in Fig. 3(a). The time delay between the power scaling down and up of the hysteresis was 20 min, which is considered more than enough for the STE to cool down and get back to its initial performance. This experiment was repeated multiple times to ensure the emitter's saturation did not cause permanent damage, which could lead to a reduction of the THz field from one measurement to the other. The thermal hysteresis graph was produced using an expanded beam to cover most of the spintronic emitter's surface with the 2D lens array. A similar experiment using a 0.01 mm^2 spherical lens showed a comparable curve recovery but with a lower power threshold.

The result of power scaling for each pump beam distribution is shown in Fig. 3(b) for the 2D lens and Fig. 3(c) for the spherical lens. In both instances, the peak-to-peak amplitude reaches saturation after a certain pump power level, beyond which the signal begins to reduce. In the case of the spherical lens, the irregular shape of the curves is of unknown origin but resembles Fig. 3(a) on the second power scaling of the thermal hysteresis. Since the saturation value remains the same in both cases, the data remains valid for comparison with the 2D lens. One of the major results is that the distributed dots of the lens array [depicted in Fig. 3(b)] improved heat dissipation, leading to a higher THz saturation point compared to an equivalent area on the spherical lens [Fig. 3(c)]. This increase in the THz field is attributed to the

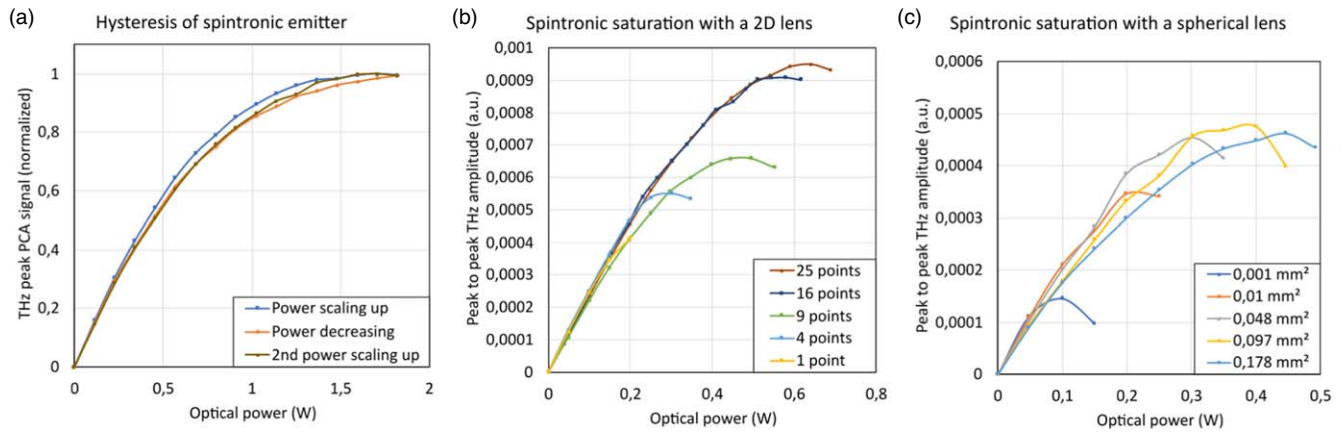

Fig. 3. Power scaling on the spintronic emitter for (a) the thermal hysteresis curve example for the spherical lens, (b) the 2D matrix lens of different sizes, and (c) the spherical lens of different sizes.

larger perimeter around the illuminated area for a similar surface, facilitating heat dissipation.

To provide a deeper understanding of the pump distribution in Fig. 2 and the data presented in Fig. 3, a comparison between surface area, maximum amplitude, number of points source, and saturation power is illustrated in Fig. 4.

As the area of the illuminated area changes based on the type of lens, the increase of the pumped surface for each size is plotted in Fig. 4(a) for the 2D lens and in Fig. 4(b) for the spherical lens. Since the area for each experiment is similar and the area increase follows a similar curve, the results of both configurations can be compared.

With similar areas however, the maximum optical pump power differs for each lens, as displayed in Fig. 4(c) for the 2D lens using more power and Fig. 4(d) for the spherical lens using less power. This behavior shows that the entire surface of the emitter is used to accumulate the thermal energy of the pump, which is distributed more efficiently with the 2D lens. Even by distributing the power over a large surface, the total size of the emitter needs to be considered to increase the saturation limit.

Figure 4(e) presents the relation between the detected THz signal at saturation and the total surface of the pump on the STE. Interestingly, when we compare the evolution of the saturation power as a function of the effective illumination area of the STE, we have a similar behavior for the 2D lens matrix and the spherical lens. However, the THz field reaches a higher saturation limit with the 2D lens matrix with up to 2 times larger field at saturation. While the configurations investigated in this research are insufficient to state the limit for the maximal surface area, it is noteworthy that the THz saturation amplitude for the spherical lens reaches a maximum at 0.097 mm^2 and then starts to decrease around 0.178 mm^2. Since the THz signal drop is not very significant, we are not sure if it is the beginning of a decrease in the THz field or if a plateau is reached. Further investigations are needed but similar conditions were met in another experiment and stated that the power should decrease for larger surface areas for a kHz repetition rate laser.[16] The reason larger surface areas were not attempted with the 2D lens is due to limitations imposed by the beam expander and the size of the 2D lens array.

Compared to previous research,[13,16,22] the saturation limit of the emitter is relatively low, with a saturation limit in the order of kW cm^{-2} at a wavelength of 1 μm and repetition rate of 80 MHz compared to an order of GW cm^{-2} in the kHz range at 800 nm.[13] This fluence saturation limit was explored recently on a fiber-tip STE, showing that higher repetition

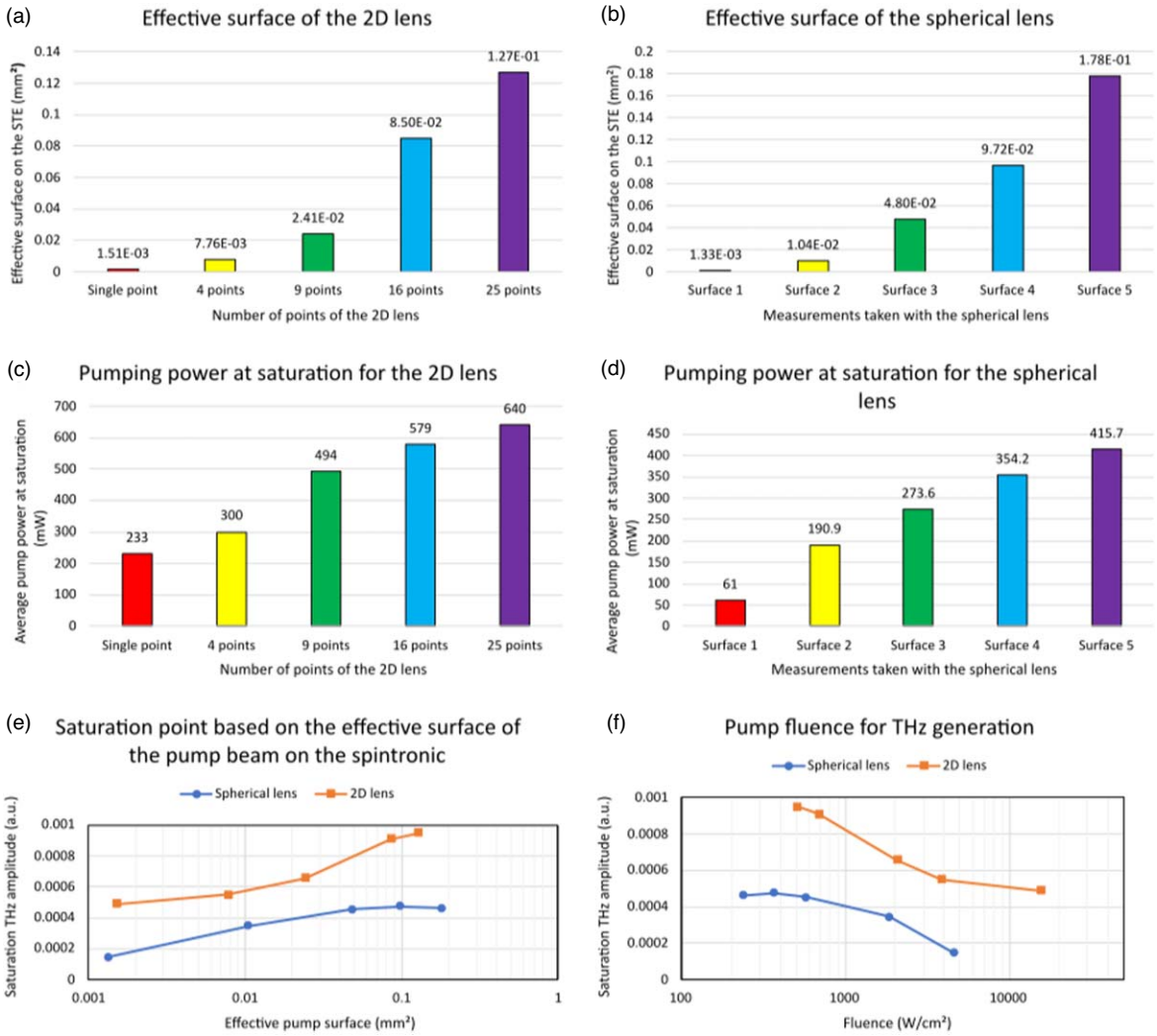

Fig. 4. Results of spatial distribution of the pump on a STE. Effective surface of the (a) 2D lens matrix and (b) spherical lens. Saturation power threshold for (c) 2D matrix lens and (d) spherical lens. (e) Comparison graph between the saturation amplitude of the THz peak-to-peak for each surface area and (f) THz generation based on pump fluence.

rate lasers will reduce the fluence saturation limit for a repetition rate of 80 MHz in the order of 70 μJ cm^{-2} at 1550 nm.[22] While the STE used in this experiment seems to reach a lower saturation limit, the relative difference between the 2D lens array and the spherical lens can be observed in Fig. 4(f). For both pumping methods, the detected THz amplitude is decreasing with an increasing fluence, but the detected signal is significantly stronger with the 2D lens. While the saturation limit drops significantly for higher fluence, the lens matrix seems to reach an asymptote for higher fluence. The findings from both the 2D matrix lens and the spherical lens confirm that a larger pump surface results in a stronger THz signal which is in adequation with other works.[16,18,19]

As the surface distribution of the pump can enhance the saturation limit of the emitter, the temporal separation of the pump pulses can increase efficiency by leaving time to dissipate the accumulated thermal energy. The optical pump energy scaling of the peak-to-peak THz pulse generated by the STE is shown for the 50% and 25% duty cycle in Fig. 5(a). As expected, the response from the STE pumped with a 25% duty cycle is less potent at low optical energy than its response when pumped with a 50% duty cycle. Since the STE saturates around 33 nJ at the 50% duty cycle, the 25% duty cycle allows an increase of the pulse energy and generation of a larger THz signal above 40 nJ. Consequently, in this configuration, the optical power, and thus, the induced thermal effect is not the same between the 25% and 50% duty cycle, despite the laser energy remaining constant. Due to this effect, the following part of the article will only consider the energy per optical pulse for the power scaling, since the average power is also affected by the duty cycle.

To better understand the effect of the duty cycle itself, Fig. 5(b) presents the behavior of the spintronic emitter at two distinct energy levels: one at 27.0 nJ selected to be below the saturation point of the 50% duty cycle optical pump, and one at 38.5 nJ above the saturation limit. As anticipated, the curve for 38.5 nJ is much more pronounced, but it also indicates a significant decrease in the efficiency of the emitter at a duty cycle higher than 35% in that specific configuration. Comparing the two energy levels reveals that the optimal duty cycle can vary for different peak powers, proving that low repetition rate and high peak optical intensity lasers are better for THz generation with an STE. This behavior is likely influenced by the spintronic saturation resistance, which depends on manufacturing methods, substrate type, and thin film optimization.

To compare the different lock-in responses of different duty cycles with the STE, Fig. 5(c) compares the previous STE response to the one obtained with a 0.9 mm thick CdTe crystal pumped with the same optical energy. Since the field of THz pulses generated from a CdTe follows a linear response to the optical pump power scaling, its response fits perfectly the theoretical curve for both pump energies, while the two spintronic responses appear to deviate at a lower modulation width for a larger energy.

Lastly, Fig. 5(d) illustrates the correlation of the curves presented in Fig. 5(c) based on the theoretical formula. This curve was calculated by reversing the theoretical equation to remove the effect due to the theoretical lock-in response proportional to sin(π·DC). By removing the sin function, the lock-in response becomes linear which helps greatly to observe from which point each emitter deviates from the theoretical curve. We observed that the CdTe emitter follows perfectly this linear theoretical response while the STE deviates at 35% and 40% duty cycle when, respectively, pumped with 38.5 and 27 nJ optical energy. Figure 5(d) shows that the curve obtained in Figs. 5(b)

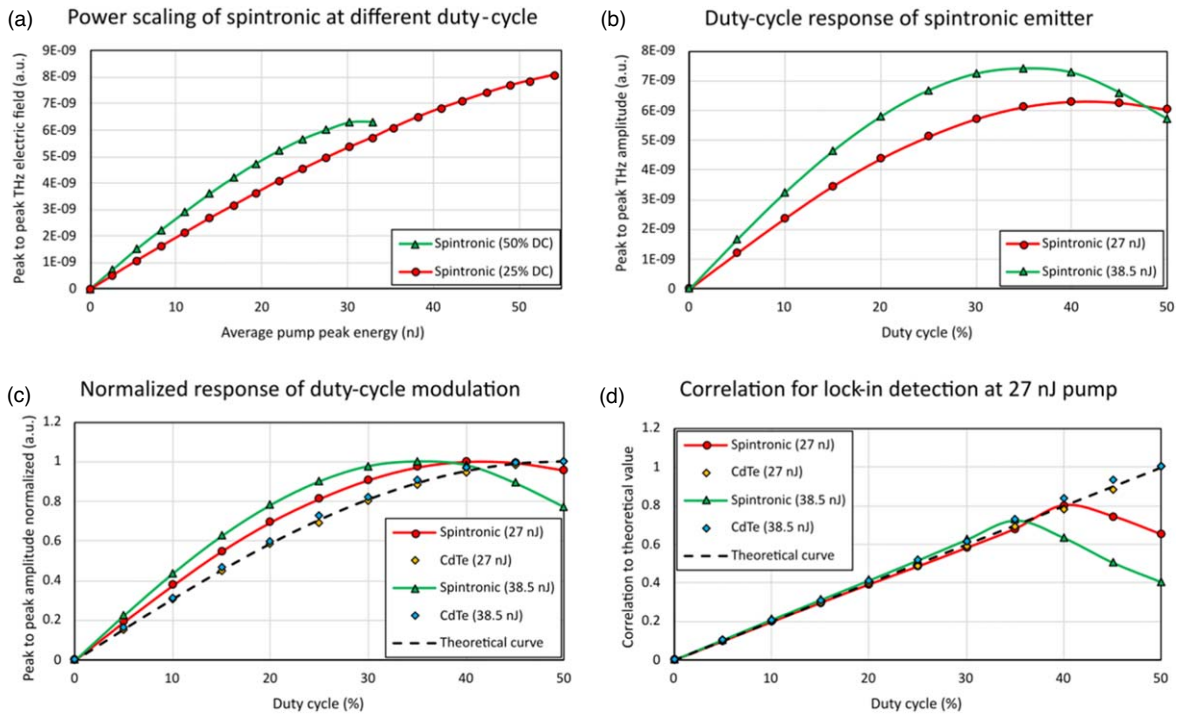

Fig. 5. THz peak-to-peak intensity for temporal distribution of the pump power on the STE. (a) Power scaling of the pump on the STE for 50% and 25% duty cycles, (b) duty cycle scaling on the STE, (c) normalized duty cycle response of the STE and CdTe, and (d) theoretical correlation with the experimental values of the CdTe and STE.

and 5(c) are caused by the lock-in detection and not a nonlinear response of the spintronic. This data suggests that the use of a shorter duty cycle is advantageous, since the maximal optical pump energy is increased before reaching the saturation regime. Consequently, the maximum generated THz signal is similarly increased despite the sine attenuation factor of the lock-in amplifier. The maximum gain from this technique varies depending on the spintronic emitter but presents an alternative solution to extend the saturation limit of the emitter by reducing the duty cycle, mimicking the behavior of a lower repetition rate oscillator laser.

In this experiment, we manipulated the spatial and temporal distribution of the optical pump from a MHz oscillator laser onto a STE to enhance its saturation limit by optimization of the heat dissipation. Using the lens matrix, we dispersed the power into multiple distinct points, effectively doubling the saturation level of the generated THz electric field of the spintronic emitter compared to a single larger point from a spherical lens. Temporally, we varied the pump energy distribution by adjusting the duty cycle of the modulation. We demonstrated that by reducing the duty cycle, the saturation limit of the STE increased allowing to use larger optical pump energy onto the STE leading to the generation and the detection of larger THZ signals. The optimal duty cycle ratio may vary for different peak energies but can be utilized beyond the known saturation limit to amplify the THz signal. This approach is particularly beneficial for enhancing the efficiency of a MHz repetition rate oscillator by emulating the relaxation time of a kHz laser. Although the lock-in detector only registers the fundamental frequency of the modulation, this method allows for the detection of stronger THz signals. These innovative solutions offer avenues to achieve higher THz generation with a MHz oscillator laser, both spatially and temporally.

Acknowledgments F. B. gratefully acknowledges financial support from NSERC Grant No. 2023-03322, and the CRC tier2 Grant No. CRC-2019-127 on Spatiotemporal encryption of THz light.We also acknowledge the financial support from the NSERC and FRQNT for Canadian and Quebec's Graduate Scholarship.

ORCID iDs François Blanchard https://orcid.org/0000-0002-3335-7458

1) M. Seo and H.-R. Park, "Terahertz biochemical molecule-specific sensors," Adv. Opt. Mater. **8**, 1900662 (2020).
2) T. Amini, F. Jahangiri, Z. Ameri, and M. A. Hemmatian, "A review of feasible applications of THz waves in medical diagnostics and treatments," J. Lasers Med. Sci. **12**, e92 (2021).
3) Q. Wang, S. Hameed, L. Xie, and Y. Ying, "Non-destructive quality control detection of endogenous contaminations in walnuts using terahertz spectroscopic imaging," J. Food Meas. Charact. **14**, 2453 (2020).
4) J. E. Nkeck, L.-P. Béliveau, X. Ropagnol, D. Deslandes, D. Morris, and F. Blanchard, "Parallel generation and coding of a terahertz pulse train," APL Photonics **7**, 126105 (2022).
5) K. B. Cooper, R. J. Dengler, N. Llombart, B. Thomas, G. Chattopadhyay, and P. H. Siegel, "THz imaging radar for standoff personnel screening," IEEE Trans. Terahertz Sci. Technol. **1**, 169 (2011).
6) A. Leitenstorfer et al., "The 2023 terahertz science and technology roadmap," J. Phys. D **56**, 223001 (2023).
7) J. Pettine, P. Padmanabhan, N. Sirica, R. P. Prasankumar, A. J. Taylor, and H.-T. Chen, "Ultrafast terahertz emission from emerging symmetry-broken materials," Light: Sci. Appl. **12**, 133 (2023).
8) C. Vicario, M. Jazbinsek, A. V. Ovchinnikov, O. V. Chefonov, S. I. Ashitkov, M. B. Agranat, and C. P. Hauri, "High efficiency THz generation in DSTMS, DAST and OH1 pumped by Cr:forsterite laser," Opt. Express **23**, 4573 (2015).
9) L. Guiramand, J. E. Nkeck, X. Ropagnol, T. Ozaki, and F. Blanchard, "Near-optimal intense and powerful terahertz source by optical rectification in lithium niobate crystal," Photonics Res. **10**, 340 (2022).
10) E. Isgandarov, X. Ropagnol, M. Singh, and T. Ozaki, "Intense terahertz generation from photoconductive antennas," Front. Optoelectron. **14**, 64 (2021).
11) T. Seifert et al., "Efficient metallic spintronic emitters of ultrabroadband terahertz radiation," Nat. Photonics **10**, 7 (2016).
12) T. S. Seifert et al., "Frequency-independent terahertz anomalous hall effect in DyCo5, Co32Fe68, and Gd27Fe73 thin films from DC to 40 THz," Adv. Mater. **33**, 2007398 (2021).
13) S. Kumar, A. Nivedan, A. Singh, Y. Kumar, P. Malhotra, M. Tondusson, E. Freysz, and S. Kumar, "Optical damage limit of efficient spintronic THz emitters," iScience **24**, 103152 (2021).
14) D. M. Nenno et al., "Modification of spintronic terahertz emitter performance through defect engineering," Sci. Rep. **9**, 13348 (2019).
15) Y. Jiang, X. Zhang, Y. Liu, P. Vallobra, S. Eimer, F. Zhang, Y. Du, F. Liu, Y. Xu, and W. Zhao, "Spintronic terahertz emitter with integrated electromagnetic control," Chin. Opt. Lett. **20**, 043201 (2022).
16) T. Vogel et al., "Average power scaling of THz spintronic emitters efficiently cooled in reflection geometry," Opt. Express **30**, 20451 (2022).
17) F. Paries et al., "Fiber-tip spintronic terahertz emitters," Opt. Express **31**, 30884 (2023).
18) T. Seifert, S. Jaiswal, M. Sajadi, G. Jakob, S. Winnerl, M. Wolf, M. Kläui, and T. Kampfrath, "Ultrabroadband single-cycle terahertz pulses with peak fields of 300 kV cm−1 from a metallic spintronic emitter," Appl. Phys. Lett. **110**, 252402 (2017).
19) R. Rouzegar et al., "Broadband spintronic terahertz source with peak electric fields exceeding 1.5 MV/cm," Phys. Rev. Appl. **19**, 034018 (2023).
20) R. Rouzegar et al., "Laser-induced terahertz spin transport in magnetic nanostructures arises from the same force as ultrafast demagnetization," Phys. Rev. B **106**, 144427 (2022).
21) P. Agarwal, R. Medwal, A. Kumar, H. Asada, Y. Fukuma, R. S. Rawat, M. Battiato, and R. Singh, "Ultrafast photo-thermal switching of terahertz spin currents," Adv. Funct. Mater. **31**, 2010453 (2021).
22) F. Paries et al., "Optical damage thresholds of single-mode fiber-tip spintronic terahertz emitters," Opt. Express **31**, 30884 (2023).
23) X. Xie, J. Xu, and X.-C. Zhang, "Terahertz wave generation and detection from a CdTe crystal characterized by different excitation wavelengths," Opt. Lett. **31**, 978 (2006).
24) X. Ropagnol, M. Matoba, J. E. Nkeck, F. Blanchard, E. Isgandarov, J. Yumoto, and T. Ozaki, "Efficient terahertz generation and detection in cadmium telluride using ultrafast ytterbium laser," Appl. Phys. Lett. **117**, 181101 (2020).
25) J. Hohlfeld, S.-S. Wellershoff, J. Güdde, U. Conrad, V. Jähnke, and E. Matthias, "Electron and lattice dynamics following optical excitation of metals," Chem. Phys. **251**, 237 (2000).